Korean J. Chem. Eng., 35(3), 725-733 (2018)
DOI: 10.1007/s11814-017-0316-6

pISSN: 0256-1115
eISSN: 1975-7220

Synthesis and characterization of low-cost ceramic membranes from fly ash and kaolin for humic acid separation

Manju Rawat and Vijaya Kumar Bulasara†

Department of Chemical Engineering, Thapar University, Patiala 147004, Punjab, India
(*Received 15 August 2017 • accepted 20 November 2017*)

Abstract−Ceramic microfiltration membranes were prepared using five different compositions formulated with different amounts of fly ash and kaolin and sintered at 900 °C. The SEM analysis evidenced a large number of small pores on the surface of kaolin-rich membranes. The M4 membrane prepared using 25% fly ash and 50% kaolin was found to be optimum as it had a good combination of pore size (0.885 μm), porosity (42.7%), mechanical strength (43.6 MPa), and chemical stability (<3% weight loss in acid and 0.02% in base), and this membrane was successfully applied in separation of humic acid from water. The permeate flux data fitted very closely with cake-filtration model, indicating the formation of a cake layer on membrane surface. Membrane fouling was found to be reversible and easily negated by cleaning and backflushing. The regenerated membrane showed better rejection of humic acid than fresh membrane with a flux recovery of above 80%.

Keywords: Ceramic Membrane, Fly Ash, Kaolin, Microfiltration, Humic Acid

INTRODUCTION

Humic acids (HA) are important organic constituents of soil and aquatic environments and are generated by chemical or microbiological degradation of organic matter [1]. They are essential components of fertilizers used to improve water holding capacity of soils. They have a complex chemical structure and cannot be represented by a molecular formula. Humic acids possess various chemically reactive functional groups such as COOH, ketonic C=O, phenolic OH and alcoholic OH. They are harmful to humans because they can interact with the red blood cells [2]. The presence of HA in water can affect its taste, odor and color; and also results in biofouling of water supply pipelines [3]. It may eventually lead to the formation of highly toxic and carcinogenic trihalomethanes and haloacetic acids during chlorination/disinfection process [4]. Hence, effective removal of HA from natural waters is very much essential prior to disinfection and supply. For this purpose, photocatalytic degradation (PCD) is a popular and widely used method for the removal of organic contaminants such as HA [5]. Besides being a slow process, the main drawback of PCD is that it produces several by-products during the reaction, which may be harmful. Therefore, membrane filtration seems to be the most suitable alterative to PCD for separation of HA from water with the advantage of recovering HA for using it as a fertilizer. The membranes are broadly classified into two types, organic (or polymeric) and inorganic (or ceramic), based on their origin/constitution.

Ceramic membranes are generally made of various inorganic materials such as silica, alumina, titania, zirconia, and kaolin. Compared to polymeric membranes, ceramic membranes possess high chemical, mechanical and thermal stability and can also withstand high temperatures and pressures. They are durable and can be regenerated. Since these membranes do not get seriously affected by the frequency and nature of cleaning, they can be subjected to aggressive cleaning agents, which is very much prevalent in industrial chemical processing units [6,7]. Since the ceramic membranes are more expensive than polymeric membranes, research is focused mainly on reducing the overall cost by using cheaper raw materials such as kaolin, clay and fly ash with low sintering temperatures (<1,000 °C) [8-10]. Kaolin is the most widely used clay mineral in the fabrication of ceramic membranes due to its high refractive properties, low cost and abundant availability [11-13].

In general, the paste method is widely used in the fabrication of ceramic membranes on a laboratory scale. Manufacturing of kaolin based ceramic membranes by paste method became popular in 2008 when Nandi et al. [10] published a paper on the preparation and characterization of cost-effective kaolin membranes. They estimated the raw-materials cost as \$130/m^2. Kaur et al. [14] studied the effects of carbonates compositions on the permeation characteristics of cost-effective ceramic membrane supports. They made kaolin-based ceramic membrane supports using different quantities of calcium and sodium carbonates. They evaluated the mean pore size and water permeability in the range of 0.3-0.8 μm and 78-1,027 $L/h \cdot m^2 \cdot bar$, respectively. They obtained high porosity, permeability and chemical stability for calcium carbonate membranes, and high pore density and mechanical strength for sodium carbonate membranes. They concluded that 20 wt% $CaCO_3$ is optimum to achieve the best membrane having 0.5 μm pore size, 37% porosity and 48 MPa flexural strength, which can be used for microfiltration of oil-in-water emulsions. It has also been reported that addition of $CaCO_3$ increases the porosity of membrane with broader pore distribution than those prepared with Na_2CO_3, and a small amount (10 wt%) of Na_2CO_3 can act as a pore modifier and results

†To whom correspondence should be addressed.
E-mail: vkbulasara@thapar.edu, vk5050@gmail.com

in small pores, whereas, excess amount (more than 20%) of Na_2CO_3 may block the pores due to the formation of sodium silicate layer [15]. To reduce the cost further, Singh and Bulasara [16] used fly ash as the main raw material in place of kaolin for economic fabrication of ceramic membranes and sintered at 800-1,000 °C. They found that the sintering temperature of 900 °C is optimum to achieve lowest mean pore size and uniform pore size distribution. They also showed the applicability of fly ash based membrane in microfiltration of oil-in-water emulsions with an oil rejection of 99.2%. Some studies [17] indicated that the particle size of raw materials controls the pore size of membrane.

In most of the studies reported in the literature, kaolin has been used as the major raw material for the fabrication of cost-effective ceramic membranes having submicron range pores. To decrease the membrane cost further, fly ash has been used as the no-cost raw material in some studies for fabrication of inorganic membranes. However, fly ash-based membranes have larger pore size, lower porosity and lower strength than kaolin-based membranes. Mixing of fly ash with kaolin may produce low cost membranes with good physical and pore characteristics. No studies have been reported on the fabrication of inorganic membranes using mixtures of fly ash and kaolin so far. Therefore, a combination of these two materials is studied in this work with an objective to reduce the cost of kaolin-based membranes without compromising upon the permeation properties and strength. An optimized membrane is also applied for separation of humic acid, an essential component of fertilizers used to improve water holding capacity of soils.

MATERIALS AND METHODS

1. Materials

The main inorganic raw materials used in this work are fly ash, kaolin, calcium carbonate, sodium carbonate, boric acid and sodium metasilicate. All chemicals were obtained from CDH India Ltd. and fly ash was collected from a local coal based thermal power plant.

2. Membrane Preparation and Characterization

Five different ceramic membranes were prepared by paste casting method with different amounts of fly ash and kaolin. The compositions of different raw materials used are shown in Table 1. First, the raw materials were accurately measured and ground properly in a ball mill. The grinding of fly ash with other raw materials takes an hour, but the grinding of kaolin powder with other raw materials takes only ten minutes. Then, a measured quantity of distilled water was used to prepare a uniform and thick paste. The paste was pressed in a circular mould of 5 mm height and 50 mm diameter. They were dried openly at ambient conditions for 12 h followed by drying at 100 °C before sintering. The membranes were then kept in a muffle furnace for heating, and the furnace temperature was slowly raised to 250 °C and again to 900 °C. After reaching the sintering temperature (900 °C), the membranes were kept for four hours and then cooled to below 100 °C. The membranes were then polished using SiC abrasive paper to achieve a flat surface and cleaned in ultrasonication bath.

Table 1. Different raw material compositions used in membrane preparation

Raw materials	Amount used (wt%) in different membranes				
	M1	M2	M3	M4	M5
Fly ash (FA)	75	50	37.5	25	0
Kaolin (KA)	0	25	37.5	50	75
$CaCO_3$	15	15	15	15	15
Na_2CO_3	5	5	5	5	5
Boric acid	2.5	2.5	2.5	2.5	2.5
Na_2SiO_3	2.5	2.5	2.5	2.5	2.5
KA/FA ratio	0 : 1	1 : 2	1 : 1	2 : 1	1 : 0

The thermo-gravimetric analysis, TGA (SII 6300, Exstar) of the raw material samples was used to determine the weight loss of samples and select appropriate sintering temperature. The X-ray diffraction, XRD (X'Pert Pro, PANalytical) analysis of sintered membranes identified various phase transformations. The scanning electron microscopy, SEM (JEOL, JSM-6510) was used to study the morphology and to check pores and defects on the surface of the membranes. The porosity was estimated by gravimetric method by soaking the membranes in water in an ultrasonic bath. The pore size and permeability of membranes were determined from water permeation experiments. The chemical stability of the membrane was checked by subjecting membranes to HCl (pH 1) and NaOH (pH 13) solutions for seven days, and the mechanical strength was determined by measuring the flexural strength of the membranes as per ASTM C1161-13 standard on a universal testing machine (Roell Z010, Zwick).

3. Permeation and Microfiltration Experiments

Water permeation tests were conducted for all the five membranes using a permeation setup consisting of a 150 mL capacity permeation cell, a flow meter, an air compressor and two pressure gauges. For each experiment, a membrane was fixed to the bottom plate of the permeation cell. Initially, the cell was filled with water and compacted for about two hours. Then, different pressures (ΔP) were applied by means of an air compressor and the corresponding flowrates of permeated water were noted for each pressure. The pore size (d_p) and permeability (L_h) were determined from water permeation plot (J_w versus ΔP) using the following correlations [12].

$$\text{Porosity, } \varepsilon = \frac{\text{pore volume}}{\text{total volume}} \tag{1}$$

$$\text{Water flux, } J_w = \frac{n\pi r^4 \Delta P}{8\mu l} = L_h \Delta P \tag{2}$$

$$\text{Pore size, } d_p = 2r = 2\times\left[\frac{8\mu l L_h}{\varepsilon}\right]^{0.5} \tag{3}$$

Here, n is the no. of pores (per m^2), μ is liquid viscosity (Pa·s) and l is membrane thickness (m). The optimized membrane (M4) was used for microfiltration experiments to separate humic acid from its aqueous solution in the same permeation setup. It has been reported that humic acid is found in surface water up to a concentration of 50 mg/L, and the environmental protection agency (EPA) has imposed a limit of 2 mg/L in drinking water [18]. In general, the particle size of humic acid ranges from 1 to 50 μm with a flaky structure. Hence, it can be separated by using microfiltration membranes. The microfiltration of aqueous solution of humic acid of

concentration 50 mg/L was at two different transmembrane pressures (1 bar and 2 bar). The humic acid concentrations in permeate were estimated from the absorbance values obtained from a UV-Vis spectrophotometer at a wavelength of 254 nm [19] with the help of a pre-calibrated curve. All experiments were conducted in triplicate.

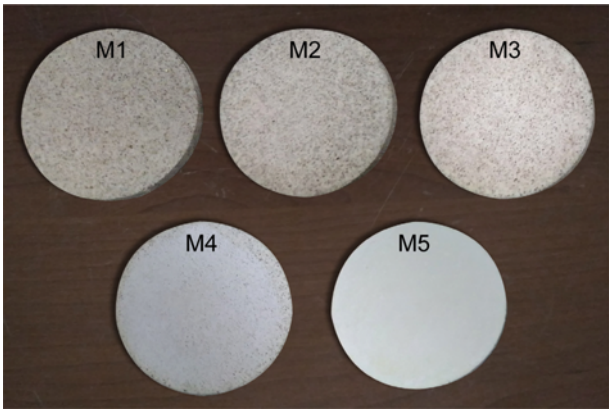

Fig. 1. Photographs of membranes of different compositions.

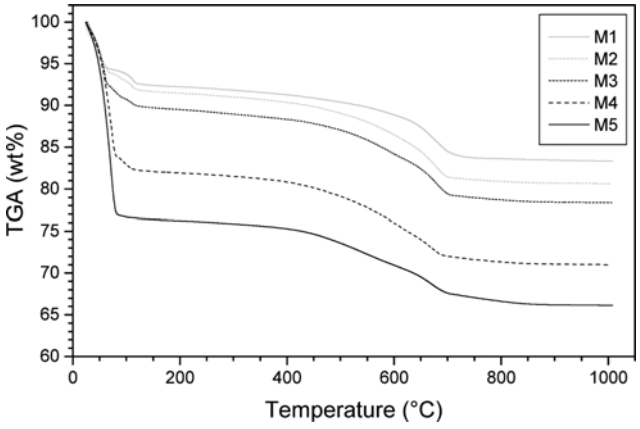

Fig. 2. TGA curves of different raw material mixtures.

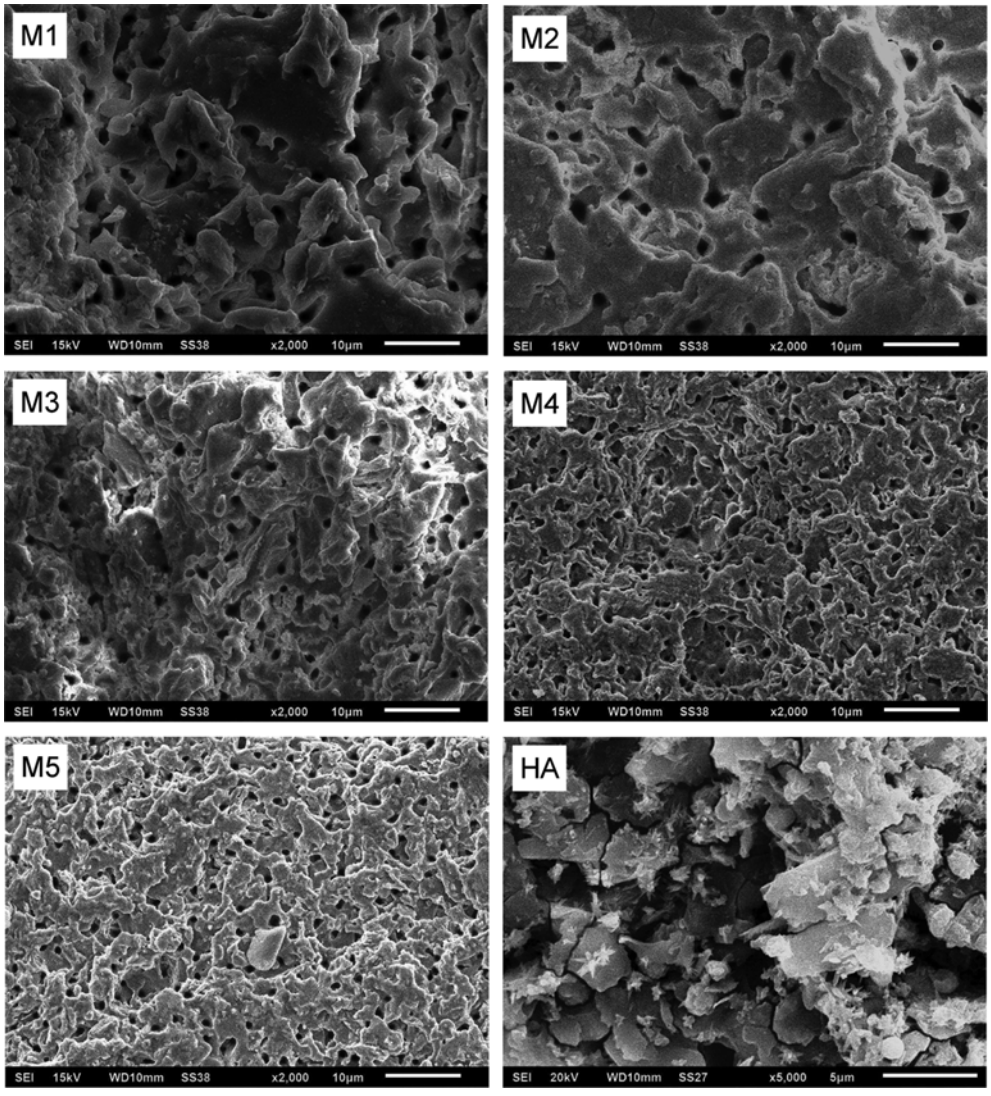

Fig. 3. SEM micrographs of different membranes (M1-M5) and humic acid particles (HA).

RESULTS AND DISCUSSION

1. Physical Observations

The physical appearance of the membranes changed with changing the composition, as shown in Fig. 1. It was noticed that the membrane made of fly ash (i.e., M1) was fully textured in greyish colour, and the one prepared using kaolin (M5) was whitish, while, those prepared using mixtures of these two materials (M2, M3, and M4) were partially textured. The surface homogeneity increased with increasing the kaolin to fly ash (KA/FA) ratio from 0 to ∞ (i.e., from 0 : 1 to 1 : 0).

2. Thermo-gravimetric Analysis

Fig. 2 shows the TGA curves of five different raw material mixtures used to prepare the membranes. As shown, the initial weight loss noticed up to 120 °C was due to the evaporation of free moisture (i.e., water added for paste making) and a little weight loss between 120 and 250 °C was due to the evaporation of bound moisture (i.e., moisture present in the particle structures of kaolin, sodium metasilicate and other raw materials). The initial weight loss was the lowest for M1 and highest for M5 as kaolin mixture requires more water to be added than fly ash mixture for making a uniform paste. The weight loss between 400 and 600 °C was due to the phase transformation of kaolin ($Al_2Si_2O_5(OH)_4$) to metakaolin ($Al_2Si_2O_7$) accompanied by release of water, which induces mechanical strength as well as porosity to the membranes. The weight loss in this region was negligible for fly ash membrane (M1), and it increased with increasing the kaolin content. Further, weight loss between 600 and 800 °C observed in all the five compositions was due to the decomposition of calcium carbonate into calcium oxide. This was accompanied by the release of carbon dioxide, which increases porosity. The total weight loss was the highest for kaolin membrane (M5) and lowest for fly ash membrane (M1).

3. Surface Morphology

The prepared membranes were analyzed by scanning electron microscopy (SEM), and corresponding images are shown in Fig. 3. The SEM pictures indicated that no cracks were present in all five membranes, and that the membrane surface is free from any defects. It can be observed that the surface morphology changed gradually with changing composition, and a small number of large pores are evident for fly ash rich membranes (M1 and M2), whereas a large number of small pores are present on the surface of kaolin rich membranes (M4 and M5). The SEM of humic acid (HA) indicates that the particles are flaky with sizes in the range 1-10 μm.

4. Particle Size Distribution of HA

The size distribution of humic acid (HA) particles was determined using a laser scattering device (Malvern, Mastersizer 2000). Fig. 4 shows the size distribution of HA particles. The majority of the particles (≈72%) were in the size range 5-10 μm. About 20% of the particles were smaller than 5 μm and only few particles (7.5%) were larger than 10 μm. The average size of humic acid particles was found to be 6.87 μm. Therefore, it can be inferred that microfiltration could be an effective method for separating HA from its solutions.

5. Phase Identification by X-ray Diffraction Analysis

X-ray diffraction (XRD) analysis was used to identify various phase transformations during the sintering process. The XRD patterns of five membranes are shown in Fig. 5, and the minerals identified are listed in Table 2. As shown, anorthite, which is formed by the interaction of CaO with alumina and silica structures during the sintering stage, is present in all the membranes in moderate amounts. The fly ash-based membrane (M1) mainly contained nacrite and dickite along with traces of mullite. The kaolin-based membrane (M5) contained metakaolinite and quartz in high amounts along with nepheline in moderate amount. However, the membranes prepared using mixtures of fly ash and kaolin (M2-M4) contained all of these minerals in different proportions. The amounts of nacrite, dickite and mullite decreased, while the amounts of meta-kaolinite, quartz and nepheline increased with increasing the kaolin/fly ash ratio (from M1 to M5). The hardness values of all these minerals are presented in Table 2.

6. Water Permeation Results

The water flux values (J_w) of different membranes at different

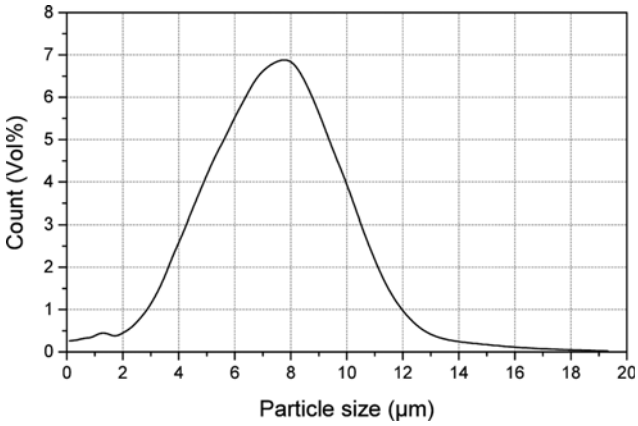

Fig. 4. Particle size distribution of humic acid.

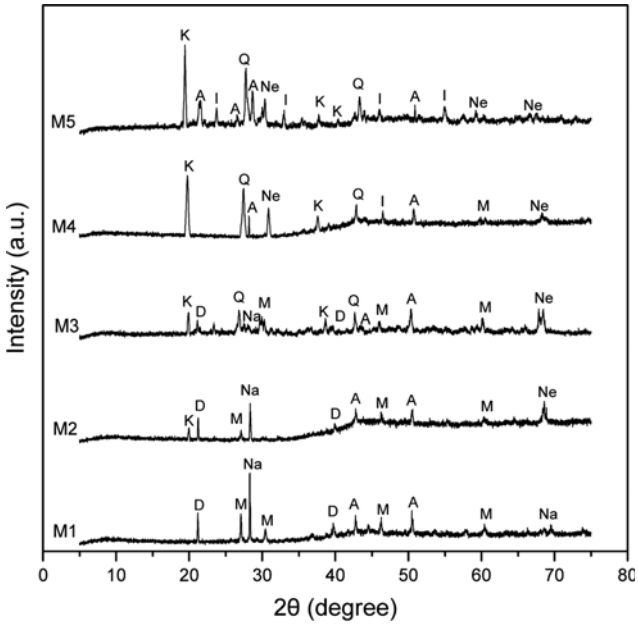

Fig. 5. XRD analysis of different membranes (M1-M5).

Table 2. List of minerals identified by XRD analysis

Notation used	Name of the mineral	Chemical formula (repeating units)	Mohs hardness (1-10 scale)
A	Anorthite	$CaAl_2Si_2O_8$	6.0
D	Dickite	$Al_2Si_2O_5(OH)_4$	1.5-2
I	Illite	$K_{0.65}Al_{2.0}[A_{l0.65}Si_{3.35}O_{10}](OH)_2$	1-2
K	Meta-kaolinite	$Al_2Si_2O_7$	4-5
M	Mullite	$Al_6Si_2O_{13}$	6-7
Na	Nacrite	$Al_2Si_2O_5(OH)_4$	2-2.5
Ne	Nepheline	$NaAlSiO_4$	6
Q	Quartz	SiO_2	7

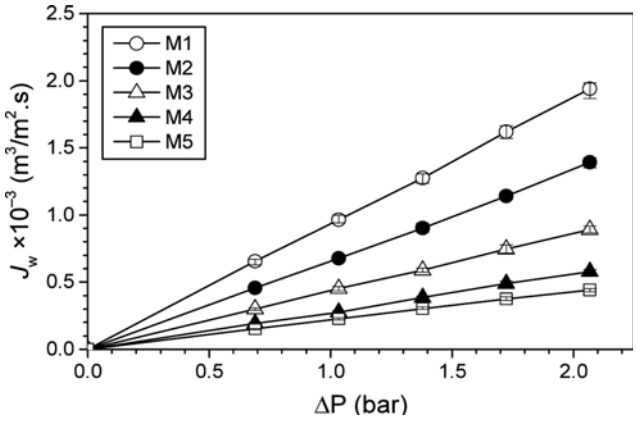

Fig. 6. Water permeation data of different membranes.

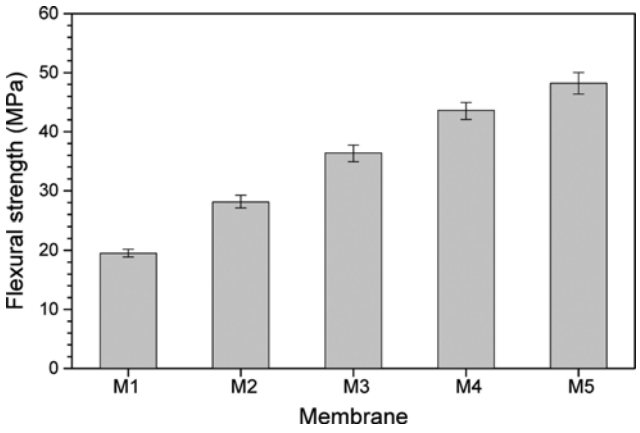

Fig. 8. Mechanical strength of different membranes.

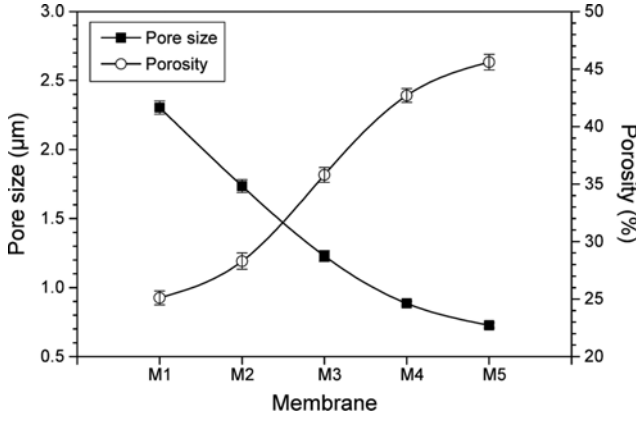

Fig. 7. Pore size and porosity versus membrane composition.

transmembrane pressures (ΔP) are shown in Fig. 6. The slopes of these plots represent the hydraulic permeability of the membranes. As shown, the permeability of membranes decreased with increasing the kaolin content. The highest value (3,369.5 L/m^2·h·bar) was oberved for fly ash-based membrane (M1) and the lowest value (780.7 L/m^2·h·bar) was observed for the kaolin-based membrane (M5). The calculated values of pore size and porosity of the five membranes are plotted in Fig. 7. As shown, the porosity was lowest for fly ash-based membrane (M1) and highest for kaolin-based membrane (M5), and it increased with increasing the kaolin content from M2 to M4. This can be correlated with the results of thermogravimetric analysis (discussed in section 3.2), which indicated maximum weight loss for M5 and minimum weight loss for M1 because of the transformation of kaolin to metakaolin accompanied by the release of water vapor. The porosity of the membranes was proportional to the total weight loss observed during the sintering process. Also, the pore size of the membranes decreased gradually with increasing the kaolin content (from 2.3 μm for M1 to 0.73 μm for M5). Therefore, it can be concluded that an increase in kaolin content leads to decrease in pore size and increase in porosity of membrane.

7. Mechanical Strength

A good ceramic membrane should have a high mechanical strength (>30 MPa) to use it as a support for ultra- and nanofiltration applications. The results (Fig. 8) showed that the mechanical strength increases proportionally with increasing the kaolin content. The fly ash-based membrane (M1) had the lowest strength (19.5 MPa) as it contained low hardness minerals nacrite and dickite (refer to XRD results discussed in section 3.4). The kaolin-based membrane (M5) had the highest strength (48.2 MPa) due to the presence of high hardness minerals metakaolin, quartz and nepheline (see Table 2). Therefore, it has been proved that the strength of a ceramic membrane depends directly on the hardness of its constituent minerals.

8. Corrosion Test Results

Fig. 9 shows the weight loss (%) of different membranes in acidic (HCl, pH=1) and basic (NaOH, pH=13) solutions. Membranes were kept in HCl and NaOH solutions for seven days to determine the chemical stability. The weight loss (%) of the mem-

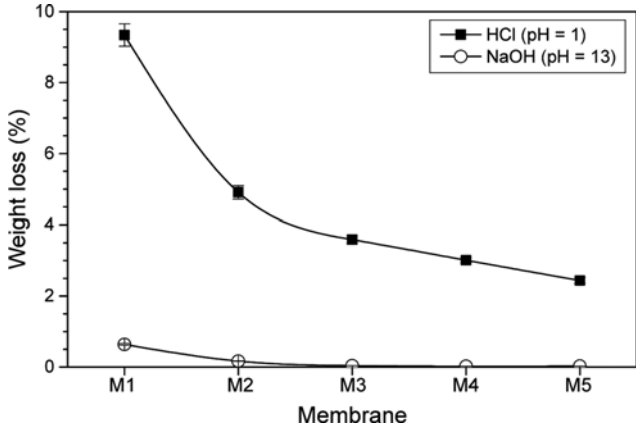

Fig. 9. Weight loss (%) versus membrane composition.

branes was determined by measuring the dry weights before and after soaking in these solutions. Fig. 9 shows that all the membranes have very good chemical stability against basic solutions, with negligible weight loss. However, in acidic solution, the weight loss of M1 and M2 (>4%) is considerably higher than that of the other membranes M3, M4 and M5. This is probably because anorthite and dickite are unstable in acidic conditions. Hence, the membranes M1 and M2 are not suitable for microfiltration of acidic solutions.

9. Selection of Optimum Composition

Based on the results discussed in the above sections, membranes M4 and M5 have desirable characteristics in terms of pore size (<1 μm), porosity (>40%), mechanical strength (>40 MPa) and chemical stability (<3% weight loss). Both these membranes are equally good. However, M4 membrane is relatively less expensive as it contains 25 wt% fly ash and 50 wt% kaolin as compared to M5 membrane, which contains 75 wt% kaolin. Therefore, the membrane M4 was chosen as the best low-cost membrane and also used for separation of humic acid from its aqueous solution.

10. Microfiltration of Humic Acid Solution

The plots of permeate flux and humic acid rejection are shown in Fig. 10. The permeate flux decreased with filtration time for both the transmembrane pressures as shown in Fig. 10(a). The observed flux decline was due to the pore blocking caused by the accumulation of humic acid particles near the pore openings. This phenomenon is quite common in dead-end filtration, as the solute particles rejected by the membrane polarize near the membrane surface. The membrane was regenerated (after using it for 20 min) by cleaning the membrane using a surfactant solution manually, followed by back-flushing with distilled water. The regenerated membrane produced a permeate flux similar to that of the original membrane with only 5% loss.

As shown in Fig. 10(b), the M4 membrane was good enough to reject more than 90% of the humic acid from its aqueous solution. The rejection values for a transmembrane pressure of 1 bar ranged between 97.1-99.8% with an average rejection of 98.46%. The average concentration of humic acid in the permeate was 0.77 mg/L. This value is well below the permissible limit for drinking water standards (i.e., 2 mg/L). Therefore, the M4 membrane prepared in this work is useful for purification of water contaminated with humic acid for drinking purposes.

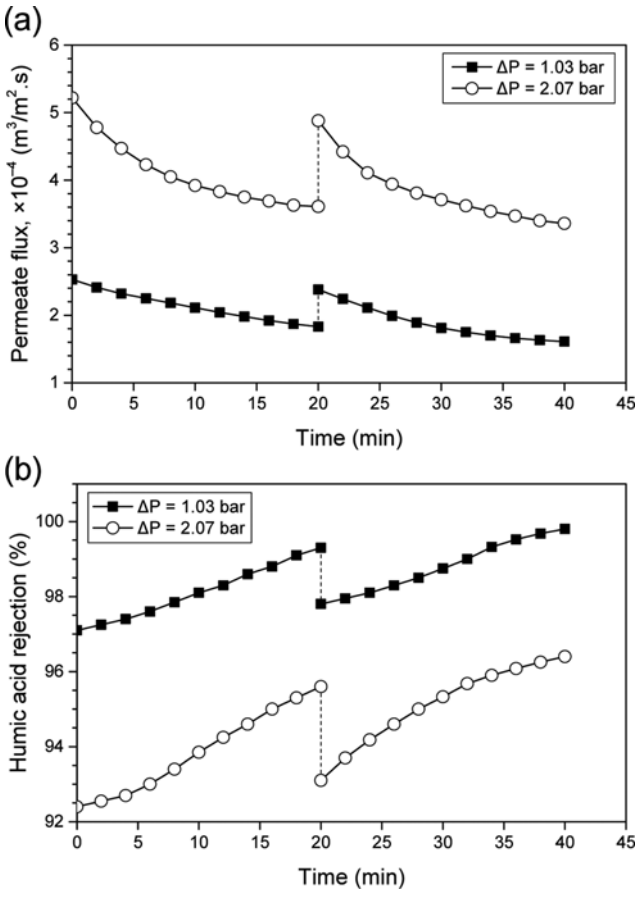

Fig. 10. Flux (a) and rejection (b) profiles observed for membrane M4.

On the other hand, the rejection values at 2 bar pressure difference ranged between 92.4-96.4% with an average rejection of 94.49%. This corresponds to an average humic acid concentration of 2.75 mg/L, which is slightly above the permissible limit. This is because of passage of solute through the membrane pores caused by breaking/folding of humic acid particles at high pressure. Although high pressure results in increase of permeate flux, it compromises upon the permeate quality. Therefore, the M4 membrane should not be used at high transmembrane pressure (2 bar).

11. Flux Decline Mechanism

The data of permeate flux (J) was analyzed using four different fouling models described in Table 3. The intermediate pore blocking (IP) model assumes that the pores of membrane are partially blocked by the particles of solute with size similar to that of pores, while the complete pore blocking (CP) model assumes that a few of the membrane pores are completely blocked by the solute particles not affecting the behavior of other pores. The standard pore blocking (SP) model assumes that the particles whose size is smaller than that of pores adsorb in the interior of pores, decreasing the effective pore size of membrane leading to flux decline. The cake filtration (CF) model assumes that the particles of solute accumulate near the membrane surface in a layer (due to their large size relative to pores), whose thickness increases with time. Further

Table 3. Model parameters of various fouling models

Model name and equation	Parameter	Values of parameters for different cases			
		ΔP=1.03 bar		ΔP=2.07 bar	
		Fresh M4	Regenerated M4	Fresh M4	Regenerated M4
Intermediate pore blocking model:	$J_{0,ip}\times10^{-4}$	2.51	2.30	4.86	4.52
$J^{-1}=J_{0,ip}^{-1}+k_{ip}t$	k_{ip}	75.4	102.6	40.9	42.4
	R^2	0.9987	0.9875	0.9735	0.9767
Complete pore blocking model:	$J_{0,cp}\times10^{-4}$	2.49	2.27	4.83	4.50
$\ln(J^{-1})=\ln(J_{0,cp}^{-1})+k_{cp}t$	k_{cp}	0.0160	0.0195	0.0169	0.0164
	R^2	0.9935	0.9736	0.9557	0.9588
Standard pore blocking model:	$J_{0,sp}\times10^{-4}$	2.50	2.28	4.84	4.51
$J^{-0.5}=J_{0,sp}^{-0.5}+k_{sp}t$	k_{sp}	0.550	0.706	0.416	0.417
	R^2	0.9966	0.9812	0.9652	0.9684
Cake filtration model:	$J_{0,cf}\times10^{-4}$	2.53	2.33	4.90	4.56
$J^{-2}=J_{0,cf}^{-2}+k_{cf}t$	$k_{cf}\times10^{5}$	7.13	10.9	1.98	2.20
	R^2	0.9997	0.9959	0.9866	0.9893

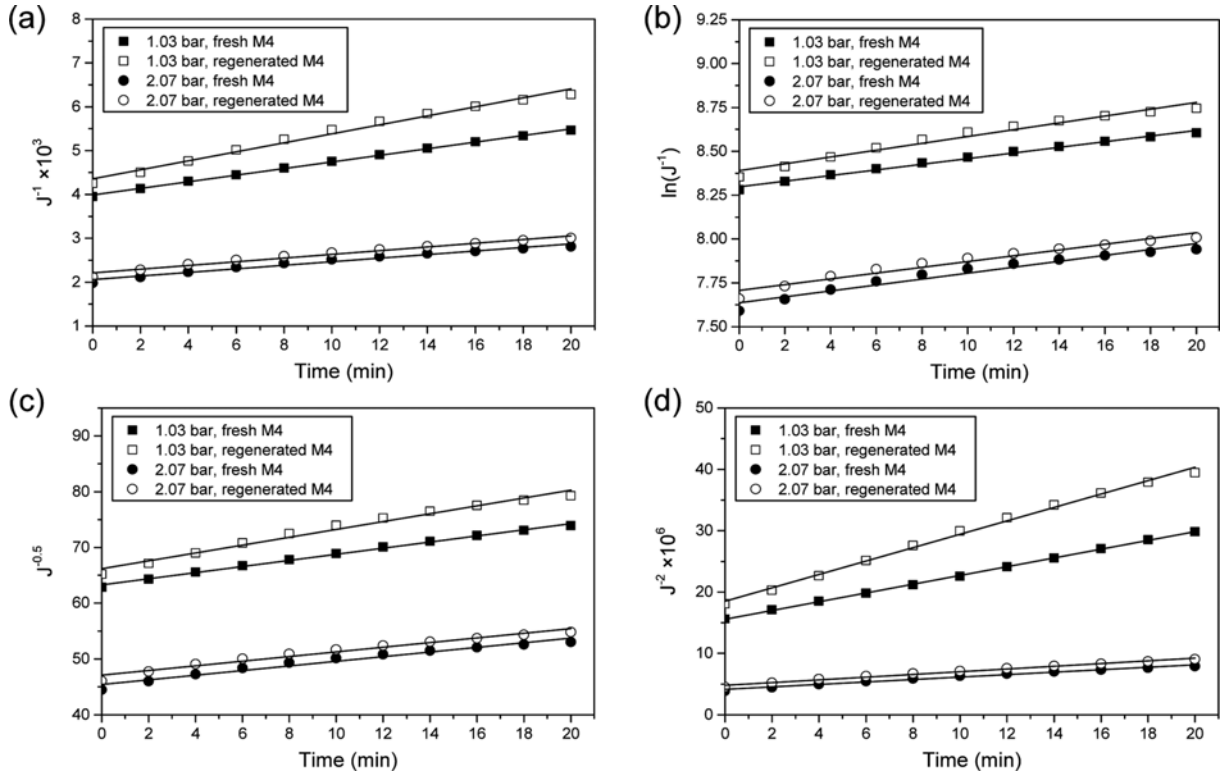

Fig. 11. Fouling models fitted to experimental data: (a) Intermediate pore blocking; (b) complete pore blocking; (c) standard pore blocking; and (d) cake filtration.

details of these models are available elsewhere [13]. As shown in Fig. 11, the fitness of the data to these models is satisfactory. However, the cake filtration model yielded the best fit to the experimental data (Fig. 11(d)). In addition, the initial flux (J_0) values found from the intercepts of the plots of Fig. 11(d) matched exactly with those observed experimentally, and the values of the coefficient of determination (R^2) were close to unity (see Table 3). Therefore, it can be inferred that the mechanism of flux decline observed during the microfiltration of humic acid (HA) is cake filtration. This implies that the particles of HA (which are larger than the pores of M4) accumulate on the surface of M4 in a layer and the thickness of the cake layer increases with time causing a significant decrease in permeate flux.

12. Fouling Resistance and Mass Transfer Coefficient

A series of resistances, namely, membrane resistance (R_m) and fouling resistance (R_f), act against the permeate transport through the membrane during filtration. The fouling resistance is composed of reversible fouling ($R_{f,rev}$), which can be eliminated by simple

Table 4. Data of steady flux and resistances for separation of HA from water by M4 membrane

Set	ΔP (bar)	Membrane type	$J_w\times10^{-4}$ ($m^3/m^2\cdot s$)	$J_{HA}\times10^{-4}$ ($m^3/m^2\cdot s$)	Flux recovery (%)	$R_{total}\times10^{11}$ (m^{-1})	$R_f\times10^{11}$ (m^{-1})
1	1.03	Fresh M4	2.89	1.83	89.91	6.35	2.33
2	1.03	Regenerated M4	2.60	1.61	83.00	7.22	2.75
3	2.07	Fresh M4	5.78	3.61	91.74	6.44	2.42
4	2.07	Regenerated M4	5.30	3.36	86.55	6.92	2.53

cleaning of membrane and irreversible fouling ($R_{f,irrev}$), which cannot be eliminated easily. The total resistance (R_{total}) is the sum of these resistances. The following correlations were used to evaluate the resistances [20].

$$R_{total}=\Sigma R=R_m+R_f=R_m+R_{f,rev}+R_{f,irrev} \tag{4}$$

$$R_{total}=\frac{\Delta P}{\mu J_{HA}};\ R_m=\frac{\Delta P}{\mu J_w};\ R_{f,irrev}=\frac{\Delta P}{\mu J_{w,regen}}-R_m \tag{5}$$

$$\text{Flux recovery}=\frac{J_{w,regen}}{J_w} \tag{6}$$

Here, J_{HA} is the steady permeate flux at the end of 20 min of HA filtration and $J_{w,regen}$ is the pure water flux after regeneration of membrane. The evaluated values of different parameters are presented in Table 4. It can be observed that the membrane M4 has very good flux recovery performance. Less than 50% of the total resistance (R_{total}) was contributed by fouling (R_f). A comparison of all three resistances is visualized in Fig. 12. The regenerated membrane offered slightly higher resistance (R_m) than fresh membrane for both transmembrane pressures. Also, the irreversible fouling resistance ($R_{f,irrev}$) caused by sorption/deposition of smaller HA particles at the interior of pore walls was insignificant when compared with the membrane resistance, but it increased after regeneration of membrane. A comparison of the two types of fouling resistances indicates that the reversible fouling (due to cake layer formation) was predominant. Although the reversible fouling resistance ($R_{f,rev}$) was significant, it can be easily eliminated by simple washing and backflushing of membrane.

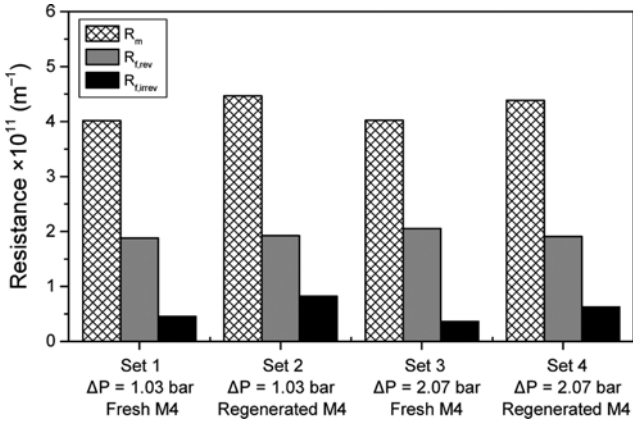

Fig. 12. Series of resistances for separation of HA and water by membrane M4.

The diffusion coefficient (D) for HA-water system was evaluated using the following equation [19].

$$D=\frac{k_BT}{6\pi\mu r_{HA}} \tag{7}$$

By substituting the values of the Boltzmann constant (k_B=1.38×10^{-23} $m^2\cdot kg\cdot s^{-2}\cdot K^{-1}$), temperature (T=298 K) and mean radius of HA particles ($r_{HA}\approx3.43\times10^{-6}$ m) and viscosity (μ=8.90×10^{-4} Pa·s), the value of D was found to be 7.138×10^{-14} m^2/s.

Concentration polarization (or accumulation of solute near membrane surface) is one of the reasons for decrease in the separation performance of a membrane. Depending on the size of solute particles, this may eventually lead to formation of a cake layer affecting the flux performance. The stagnant film model [21] is universally used to describe the concentration polarization in various pressure driven membrane processes. Hence, the mass transfer coefficient (k) was evaluated as follows [21].

$$J=k\ln\left(\frac{C_m-C_p}{C_b-C_p}\right) \tag{8}$$

$$\ln\left(\frac{C_p}{C_b-C_p}\right)=\ln\left(\frac{C_p}{C_m-C_p}\right)+b\left(\frac{J}{u^{0.33}}\right) \tag{9}$$

$$\text{True rejection, } R=1-\frac{C_p}{C_m} \tag{10}$$

$$\text{Thickness of cake layer, } \delta=\frac{D}{k} \tag{11}$$

Here, C_b, C_p and C_m, are concentration of HA in bulk solution (feed), permeate and at the membrane surface, respectively, and u is the flow velocity of permeate through the membrane. The evaluated values of all parameters are presented in Table 5. The true

Table 5. Mass transfer coefficient for separation of HA from water by M4 membrane

Set	ΔP (bar)	Membrane type	b	R	C_m (mg/L)	δ (nm)	$k\times10^{-5}$ (m/s)
1	1.03	Fresh M4	2075	0.9999	210	1.70	4.167
2	1.03	Regenerated M4	2627	1.0000	693	2.33	3.280
3	2.07	Fresh M4	472	0.9909	417	0.35	23.83
4	2.07	Regenerated M4	673	0.9965	991	0.51	15.97

rejection was found to be close to 100%. The thickness of the cake layer was in the range 0.35-2.33 nm and the concentration of HA at the membrane surface (C_m) was in the range 210-991 mg/L. For a high transmembrane pressure (ΔP=2.07 bar), the cake layer thickness (δ) was lower and the concentration of HA (C_m) was higher than that for the other case (ΔP=1.03 bar) because of high applied pressure. Higher value of C_m could be the reason for the lower solute rejection observed at high ΔP. The mass transfer coefficient (k) values were higher for high ΔP due to high flux. Lower values of k for regenerated membrane indicate decrease of permeate flux. The values of k observed in this work for microfiltration of HA are higher than that observed for a cellulose ultrafiltration (UF) membrane in literature [19]. Therefore, it can be concluded that the membrane M4 has superior flux performance in separation of HA from water than cellulose based UF membrane.

CONCLUSIONS

Ceramic microfiltration membranes were prepared using five different compositions formulated with different amounts of fly ash and kaolin. With the help of TGA of the raw material mixtures, the sintering temperature was selected as 900 °C. It was also observed from the TGA that the weight loss during the sintering process increases with increasing the kaolin content due to release of water in the transformation of kaolin to metakaolin. The SEM analysis of the sintered membranes evidenced a large number of small pores on the surface of M4 and M5 membranes. The size distribution of humic acid particles revealed that the majority of the particles were of the size 5-10 μm and the average particle size was 6.87 μm. The XRD analysis revealed the presence of metakaolin, quartz and nepheline in kaolin rich membranes. The water permeation study indicated that the porosity of the membranes increases and pore size decreases with increasing the kaolin content in the raw materials mixture. The mechanical strength and chemical stability also increased with increasing the kaolin content. The M4 membrane composition (25% fly ash and 50% kaolin) was selected as optimum as it resulted in a good combination of pore size (0.885 μm), porosity (42.7%), mechanical strength (43.6 MPa), and chemical stability (<3% weight loss in acid and 0.02% in base). Aqueous solution of humic acid was prepared with a concentration of 50 mg/L and used as feed for microfiltration experiment with M4 membrane at two different transmembrane pressures (1 bar and 2 bar). It was noticed that a pressure difference of 2 bar results in superior flux, while, a pressure difference of 1 bar results in better rejection of humic acid (98.46%) and good permeate quality (0.77 mg/L). Therefore, the membrane M4 has been successfully applied in the separation of humic acid from water. Fouling study indicated that the mechanism of size exclusion based pressure driven microfiltration of HA was cake layer formation caused by concentration polarization. The resistance to permeate flow was mainly offered by reversible fouling, which was effectively eliminated by membrane regeneration through cleaning and backflushing after 20 min of use. High flux recovery values (>80%) indicated superior performance of M4 membrane.

REFERENCES

1. L. Wang, C. Han, M. N. Nadagouda and D. D. Dionysiou, *J. Hazard. Mater.*, **313**, 283 (2016).
2. S. Javdaneh, M. R. Mehrnia, and M. Homayoonfal, *Korean J. Chem. Eng.*, **33**, 3184 (2016).
3. F. S. Dehkordi, M. Pakizeh and M. Namvar-Mahboub, *Appl. Clay Sci.*, **105**, 178 (2015).
4. A. L. Ahmad, A. A. Abdulkarim, S. Ismail and O. B. Seng, *Korean J. Chem. Eng.*, **33**, 997 (2016).
5. K. Szymański, A. W. Morawski and S. Mozia, *Chem. Eng. J.*, **305**, 19 (2016).
6. Y. Zou, H. Jiang, H. Gao and R. Chen, *Korean J. Chem. Eng.*, **33**, 2453 (2016).
7. S. Jana, A. Saikia, M. K. Purkait and K. Mohanty, *Chem. Eng. J.*, **170**, 209 (2011).
8. B. Das, B. Chakrabarty and P. Barkakati, *Korean J. Chem. Eng.*, **34**, 2559 (2017).
9. C. M. Kaniganti, S. Emani, P. Thorat and R. Uppaluri, *Sep. Sci. Technol.*, **50**, 121 (2015).
10. B. K. Nandi, R. Uppaluri and M. K. Purkait, *Appl. Clay Sci.*, **42**, 102 (2008).
11. B. K. Nandi, B. Das, R. Uppaluri and M. K. Purkait, *J. Food Eng.*, **95**, 597 (2009).
12. S. Emani, R. Uppaluri and M. K. Purkait, *Desalination*, **341**, 61 (2014).
13. B. K. Nandi, R. Uppaluri and M. K. Purkait, *Sep. Sci. Technol.*, **44**, 2840 (2009).
14. H. Kaur, V. K. Bulasara and R. K. Gupta, *J. Ind. Eng. Chem.*, **44**, 185 (2016).
15. H. Kaur, V. K. Bulasara and R. K. Gupta, *Desalin. Water Treat.*, **53**, 1204 (2016).
16. G. Singh and V. K. Bulasara, *Desalin. Water Treat.*, **53**, 1204 (2013).
17. S. Jana, M. K. Purkait and K. Mohanty, *Sep. Sci. Technol.*, **46**, 33 (2011).
18. J. S. Kamyotra, *Pollution control acts, rules and notifications issued thereunder*, 6th Ed., Central Pollution Control Board, India (2010).
19. N. Shamsuddin, D. B. Das and V. M. Starov, *Chem. Eng. J.*, **276**, 331 (2015).
20. A. L. Ahmad, A. A. Abdulkarim, S. Ismail and B. S. Ooi, *Sep. Sci. Technol.*, **54**, 3257 (2015).
21. A. L. Zydney, *J. Membr. Sci.*, **130**, 275 (1997).